State-to-state scattering of metastable CO molecules from a LiF (100) surface

Rienk T. Jongma, Giel Berden, and Theo Rasing
Research Institute for Materials, University of Nijmegen Toernooiveld, 6525 ED Nijmegen, The Netherlands

Helmut Zacharias
Research Institute for Materials, University of Nijmegen Toernooiveld, 6525 ED Nijmegen, The Netherlands and Physikalisches Institut, University of Münster Wilhelm-Klemm-Str. 10, 48149 Münster, Germany

Gerard Meijer
Research Institute for Materials, University of Nijmegen Toernooiveld, 6525 ED Nijmegen, The Netherlands

(Received 29 January 1997; accepted 24 March 1997)

Scattering of electronically excited, state-selected metastable CO($a^3\Pi$) molecules from a cleaved LiF(100) surface is studied experimentally. Internal state distributions, fluorescence profiles, time-of-flight (TOF) profiles and angular distributions of the surviving metastable CO molecules are measured. Relative and absolute survival probabilities are determined for various impact velocities. The dependence of translation and rotational temperature on the velocity of the incoming beam unambiguously indicates a direct inelastic scattering process, even though the angular distributions are broad, both in plane and out of plane. The internal state distribution after scattering shows an overpopulation of the initially prepared $\Omega=1$-component relative to the other spin components. [S0021-9606(97)00125-6]

I. INTRODUCTION

During the last decades many experiments on molecular beam-surface interaction have been performed.[1,2] These experiments almost exclusively utilize molecules in their electronic and vibrational ground state. Measuring the velocity distribution, angular distribution, and internal state distribution of the scattered molecules for known parameters of the incoming beam and for a known scattering geometry, yields detailed information on the molecule-surface interaction potential.[3–7]

A few groups have reported on scattering experiments in which vibrationally excited molecules are used[8–11]. So far, little is known about the interaction of electronically excited molecules with surfaces; the study of electronically excited molecules colliding with surfaces is thus far limited to molecules residing in the different Ω components of the electronic ground state.[12–14]

A variety of scattering experiments with metastable atoms have been performed, mostly focused on the electronically inelastic channels of the scattering process. This has led, among others, to the development of metastable atom deexcitation spectroscopy (MDS/MIES) as a surface spectroscopic tool.[15,16]

Recently the first scattering experiments with electronically excited CO molecules have been realized.[17] In this paper we report in more detail on the state-to-state surface scattering experiment with quantum-state selected metastable CO molecules. By studying the electronically elastic channel only, the elastic scattering properties of the process are probed; each molecule being trapped or chemisorbed will be electronically deexcited and removed from the measured signal. Apart from information obtained from time-of-flight (TOF) and angular distributions of the surviving metastable molecules, additional information concerning the interaction potential can be extracted from the internal state distribution of the scattered molecules.

II. EXPERIMENT

The experimental setup consists of a pulsed molecular beam machine connected to an ultrahigh vacuum (UHV) system. A schematic view of this machine is presented in Fig. 1. Its operation has been described in detail earlier.[18] To summarize, the two differentially pumped chambers of the molecular beam machine are connected by a 0.8-mm-diam skimmer. The source chamber contains a pulsed valve (R.M. Jordan Co.) with a 0.35 mm orifice. In the experiments a mixture of 20% CO seeded in neon, argon, krypton or xenon is expanded from the nozzle, providing a supersonic beam of gas pulses with a duration of typically 20–30 μs. Different seeding gasses are used to vary the mean velocity of the CO molecules in the molecular beam. About 2 cm downstream from the nozzle the rotationally cold CO molecules are excited from the electronic ground state to the $a^3\Pi_1(v=0, J=1)$ level by direct laser excitation. To be able to focus the metastable CO molecules with a hexapole, the upper component of the $J=1$ Λ doublet in the $a^3\Pi_1(v=0)$ state is populated via excitation on the $Q_2(1)$ line of the spin-forbidden $a^3\Pi(v=0)\leftarrow X^1\Sigma^+(v=0)$ transition (around 206 nm[19]) using pulsed laser radiation.

This laser light is produced with an argon-ion laser (Spectra Physics 2017) pumped cw-ring dye laser system (Spectra Physics 380), running on a mixture of DCM and Rhodamine 6G, that produces 100 mW of 618 nm laser light in a 1 MHz bandwidth. The output of the cw laser is amplified in a Nd:YAG laser (Spectra Physics GCR 190) pumped pulsed dye amplified system (Lambda Physik LPD3000) run-

 0021-9606/97/107(1)/252/10/$10.00

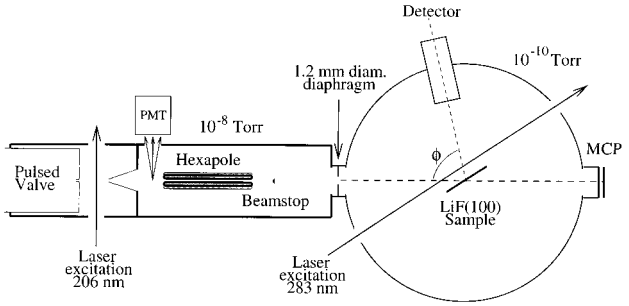

FIG. 1. Schematic view of the experimental setup, consisting of a pulsed molecular beam machine connected to an UHV scattering chamber. The 206 nm laser excitation in combination with the hexapole-beamstop-diaphragm setup allows preparation of a pure beam of metastable CO molecules in the UHV chamber. The production of metastable CO molecules is monitored in the hexapole chamber with the PMT. The TOF profile of the incoming beam is measured with the MCP in the UHV chamber. Direct detection of metastable CO molecules, detection of fluorescence photons, or ions prepared by the 283 nm laser is realized with several detection schemes as displayed in more detail in Fig. 2.

ning on sulforhodamine 640. The pulsed laser radiation around 618 nm is frequency tripled in the combination of a KDP and a BBO crystal. The 206 nm laser light that is obtained (0.5 mJ in a 150 MHz bandwidth), is separated from the fundamental and second harmonic using a number of 45° mirrors for 206 nm laser light ($R>98\%$, Laseroptik GmbH). The favorable spectral brightness of this laser system, as compared to normal pulsed dye lasers, allows efficient pumping on the $a^3\Pi \leftarrow X^1\Sigma^+$ transition.

After the molecular beam is skimmed, it enters the hexapole chamber. In this chamber a photomultiplier (PMT) is monitoring the $a \rightarrow X$ fluorescence of metastable CO molecules that pass through its field of view. This PMT is mounted perpendicular to the molecular beam axis, 7.5 cm downstream from the excitation region. The fluorescence signal is used to optimize spatial alignment and frequency of the excitation laser, and can be used as a reference for the number of metastable molecules present in the molecular beam. The hexapole chamber contains a 15-cm-long electrostatic hexapole state selector as well as a 1.2-mm-diam beamstop blocking the central part of the beam. A 1.2-mm-diam diaphragm, connecting the hexapole chamber to the UHV system, is mounted in the ''shadow'' of the beamstop. The beamstop thereby prohibits the unfocused molecular beam from entering the UHV system.

Metastable CO molecules in the upper Λ-doublet component with $M\Omega=-1$ (prepared by laser excitation on the $Q_2(1)$ transition) can be focused by the electrostatic hexapole state selector based on the first order Stark effect.[2,20] The voltage on the hexapole is optimized to bend molecules with a certain velocity in this specific quantum state around the beamstop and focus them precisely at the location of the opening of the diaphragm, as experimentally demonstrated earlier for this system.[18] The combination of hexapole, beamstop and diaphragm thus transmits an almost pure beam of metastable CO molecules in a single quantum state to the UHV system, in principle free of ground state CO and carrier gas atoms. Less than 1% of the ground state CO molecules and of the carrier gas atoms will enter the UHV system.

In the center of the UHV system, 72.5 cm downstream from the excitation region, a LiF sample is mounted on an X,Y,Z manipulator. The manipulator also allows rotation of the sample around a vertical axis, thereby varying the angle of incidence. The LiF surface is chosen for these experiments as it is a likely candidate for which the internal energy of the metastable CO molecules (6.0 eV) will not be lost during the interaction.

The LiF sample is obtained from a 10×10 mm^2 rod of single crystalline LiF. The LiF samples are cleaved along the (100) direction, which is the only stable direction for cleaving, to provide an atomically flat surface. Cleaving is done under atmospheric conditions since there appear to be no differences between air-cleaved and vacuum-cleaved samples used in similar experiments.[11,21] Within 10 min after cleavage the sample is mounted and put in the UHV chamber, which is subsequently pumped down. After bakeout a base pressure of 2×10^{-10} Torr is obtained. The LiF sample is heat cleaned in UHV for a period of 2 h at 600 K, and kept at room temperature during the experiments. For a few samples the flatness of the surface was checked after the experiments (in open air) with an atomic force microscope. The resulting images show large terraces with a typical width of a few μm. The data presented here are reproduced in experiments with many different LiF samples.

A. Detection schemes

Direct detection of the metastable CO molecules is performed with microchannel plate (MCP) detectors which allow both time- and spatially resolved detection[18]. The detection efficiency for $a^3\Pi(v=0)$ CO is approximately 6×10^{-4}. This method is not quantum-state specific and is based on detection of electrons produced by Auger deexcitation. In the emission process the electronic energy of the metastable CO molecule (6.0 eV) is used to create electrons at the surface of the MCP detector, and these electrons are subsequently detected. The detection efficiency is therefore not expected to depend strongly on the internal and kinetic energy of the detected molecules. Similar detection schemes have been shown to be essentially independent of kinetic energy.[22–25] Furthermore, the MCP detector has been used earlier to measure excitation spectra in a molecular beam.[18] Rotational levels up to $J=8$ could be measured for CO molecules in the $a^3\Pi$ state, and could be fitted using a single rotational temperature, indicating that at least up to $J=8$ the effect of rotational energy on the detection efficiency can be neglected. If, however, part of the internal or kinetic energy can be used as well for the production of Auger electrons, the detection efficiency still would show only a minor dependence on these quantities as it is only a small contribution ($\leqslant$ 0.1 eV) to the 6.0 eV of electronic energy of the metastable CO molecules.

TOF profiles of the incoming metastable CO beam are monitored with a double staged, 25-mm-diam MCP detector (Fig. 1) when the LiF surface is moved out of the beam. This detector is mounted 98 cm downstream from the excitation

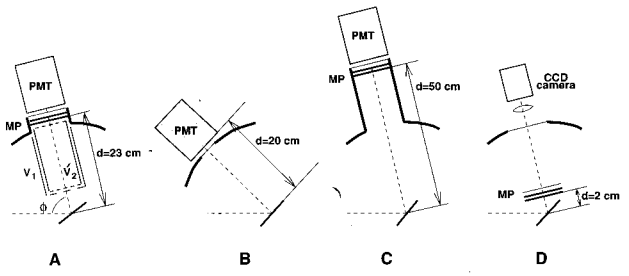

FIG. 2. Detailed view of the detection system in the UHV system: (a) REMPI spectra are obtained using the ion extraction assembly mounted in front of a fast MCP/phosphor screen (MP) detection system. The (spatially integrated, time-resolved) emission of the phosphor screen is detected with a PMT. The extraction unit consists of two concentric tubes with extraction grids mounted at the end. The axis of the incoming metastable CO beam and the axis of detection enclose a fixed angle of $\phi=72°$. (b) Spontaneous emission of incoming and scattered beam is monitored with a PMT directly looking at the fluorescence signal of the metastable CO molecules ($\phi=36°$). (c) TOF profiles of scattered metastable CO molecules are detected with the same PMT-MCP/phosphor screen combination as shown in a, allowing direct detection of the metastable CO molecules ($\phi=72°$). (d) Angular distributions of the scattered metastable CO molecules are measured, using a CCD camera system looking (time-integrated, spatially resolved) at the emission of a MCP/phosphor screen combination similar to the one mentioned above.

region, and allows determination of the parallel velocity distribution of the incoming beam of metastable CO molecules.

The internal state distribution of the incoming and the scattered metastable CO beam is probed via one-color (1 +1)-resonance enhanced multiphoton ionization (REMPI) and mass-selective ion detection. The ions are produced by a laser that is resonant with the $b^3\Sigma^+(v=0)\leftarrow a^3\Pi(v=0)$ transition around 283 nm.[26,27] This laser is a Nd:YAG pumped pulsed dye laser system (Spectra Physics GCR-3/PDL-2 combination) running on fluorescein 548. The output of this laser is frequency doubled in a KDP crystal, producing 10 mJ of 283 nm radiation with a bandwidth of 0.4 cm^{-1}. The laser intensity is approximately 100 times more than needed to saturate the b←a transition. For this reason the recorded spectra directly reflect the population in the $a^3\Pi$ state, and Hönl–London factors can be omitted in the analysis. The laser beam is running parallel to the LiF surface through the UHV machine, at a distance of 5 mm from the surface (see Fig. 1).

The laser-produced ions are accelerated in the direction of a fast 25-mm-diam MCP/phosphor screen (with a 80 ns decay time to 10% of peak signal) combination using the optional ion-extraction assembly (Fig. 2a). The extraction assembly consists of two concentric tubes. The inner tube has two parallel grids mounted at both ends, thereby creating a field-free TOF region of 19 cm for the laser produced ions. The outer tube is open at the side of the detector and has a grid mounted 3.2 cm away from the center of the LiF surface at the other side. The distance between the extraction grids of outer and inner tube at the side of the LiF sample is 3 mm.

At the end of the ion-extraction assembly the ions are accelerated toward the MCP/phosphor screen combination which is mounted 5 mm away from the end of the TOF tube. The total distance between LiF surface and MCP is 23 cm. The (spatially integrated) emission of the phosphor screen is detected time resolved with a PMT. The front of the MCP is biased at −1400 V. The voltage on the outer tube is $V_1=-20$ V, the voltage applied to the inner tube is $V_2=-600$ V. The mount of the LiF sample is grounded during all the experiments. The voltages on the ion-extraction assembly are chosen to optimize the time separation between ions produced from the incoming and from the scattered beam. For the scattered molecules the velocity component in the direction of the MCP detector is much larger than for the molecules in the incoming beam. A low voltage on the first extraction grid (V_1) makes use of this difference to obtain an almost complete time-separation between the two signals. A high voltage on the second electrode (V_2) gives rise to rather narrow ions peaks. In this detection scheme, the ions produced from the scattered beam arrive earlier on the detector than ions produced from the incoming beam, and can be sensitively detected. On resonance the ion signal of the incoming beam is a few orders of magnitude larger than the signal of the scattered beam and would, without this scheme, overwhelm the scattering signal.

The axis of the incoming beam of metastable CO molecules and the axis of detection of the scattered molecules enclose a fixed angle of $\phi=72°$ ($\phi=\theta_i+\theta_f$, with θ_i (θ_f) the angle enclosed by the surface normal and the incoming (scattered) beam) in this setup. The LiF sample is rotated to make an angle of incidence of $\theta_i=51°$ with the incoming metastable CO beam, allowing free passage of the REMPI laser, close to the LiF surface. The diameter of the laser beam is 6 mm, to probe scattered molecules in a rather large volume.

The spontaneous emission of the metastable CO molecules can be monitored with a PMT in the UHV chamber as well (Fig. 2b), allowing an estimation of the upper limit of the absolute survival probability by comparing the fluorescence signal of incoming and scattered metastable CO molecules. The PMT is mounted at a distance of 20 cm from the LiF(100) surface. The detection angle $\phi=36°$. The fluorescence profiles of the metastable CO molecules are recorded for the specular direction ($\theta_i=\theta_f=36°$). Fluorescence profiles are measured with the LiF sample placed in the beam of metastable CO molecules and with the molecular beam hitting the stainless steel sample holder under otherwise identical circumstances. Stainless steel efficiently deexcites the metastable CO molecules and the thus recorded fluorescence profile will not contain a contribution of the fluorescence signal of the scattered molecules.

TOF profiles of the scattered metastable CO molecules are recorded by the PMT, registering the time-resolved and spatially integrated emission of the MCP/phosphor screen combination, located 50 cm away from the LiF surface (Fig. 2c, $\phi=72°$). Molecules scattering in the specular direction are monitored ($\theta_i=\theta_f=36°$) to allow direct comparison with the fluorescence profiles.

Angular distributions of the scattered molecules are measured with a charge-coupled device (CCD) camera system recording the time-integrated emission of another 25-

mm-diam MCP/phosphor screen detector, similar to the one mentioned above, but this time mounted 2 cm away from the LiF surface (Fig. 2d). The camera system has a gated image-intensifier which is at high voltage during typically 100 μs, corresponding to the width of the arrival time distribution of the metastable CO beam at the detector.

B. Data acquisition

The signals recorded by the MCP (Fig. 1) or PMT (Fig. 2) are fed into a digital oscilloscope with a 10 bit vertical resolution (Lecroy 9430), where they are digitized and then read out by a computer (486PC) via a GPIB interface (National Instruments). The TOF profiles of the incoming beam are measured by summing the detected signal over typically 1500 shots in the 16 bit memory of the oscilloscope and by subsequent transfer to the PC.

The fluorescence profiles and TOF profiles of the scattered molecules are measured using time-resolved event counting. These signals are too low to average directly on the oscilloscope. Therefore the signal is typically summed over 120 shots in the memory of the oscilloscope and read out by the computer. The maximum of a certain signal peak that appears above a preset threshold is counted as a single event (detection of a metastable molecule or a photon) and put into a data array in the computer at a position corresponding to the detection time. The length of the time interval over which the number of events is summed can be chosen afterward.

The use of the PMT or PMT-MCP/phosphor screen combination guarantees sensitive detection of single events due to the large amplification that can be obtained. The MCP/phosphor screen combination together with the CCD camera system (LaVision Flamestar) allows spatially resolved detection of single metastable CO molecules with a signal to noise ratio better than 100. The software to control and read out the CCD camera can be used for two-dimensional (2D) event counting. The detected angular distribution is therefore free of noise caused by the dark current of the CCD chip.

The REMPI spectra are measured with the same detection system, allowing sensitive detection of ions. The signal is summed over typically 25 laser shots on the oscilloscope and read into the computer. The signal in a preset time-gate (corresponding to the arrival time of the ions) is averaged and recorded after subtraction of the baseline. The energy of the ionization laser and the amount of metastable CO molecules in the beam, the latter monitored via the fluorescence signal on the PMT in the hexapole chamber, are recorded simultaneously with the ion signal. The fluorescence signal is averaged on a gated integrator/boxcar averager (Stanford Research Systems (SRS) 250) because of the large time delay between the fluorescence signal and the ion signal (on the order of a ms), and because of the presence of only two channels on the oscilloscope. The averaged output of the boxcar is digitized by a 13 bit digitizer (SRS 245) and read into the computer together with the oscilloscope signals. Thus recorded REMPI spectra can be corrected for intensity fluctuations in the beam of metastable CO molecules and for fluctuations in the energy of the ionization laser.

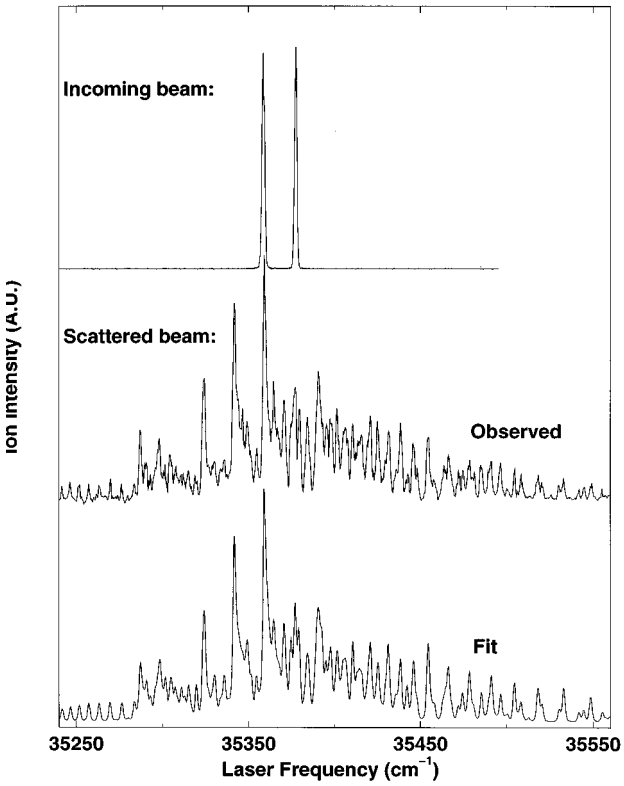

FIG. 3. Upper trace: REMPI spectrum reflecting the internal state distribution of the incoming beam. The two peaks both originate from the + parity component of the $J=1$ level in the $a^3\Pi_1(v=0)$ state. The experimental spectra are recorded for a gas mixture of 20% CO in Ar. Middle trace: REMPI spectrum which reflects the internal state distribution of scattered metastable CO molecules. This spectrum is recorded for $\theta_i=51°$. Lower trace: Best fitting spectrum using a rotational temperature of 293 K, and an overpopulation of the $\Omega=1$ component with a factor 2.5 relative to the other Ω components.

Synchronization of pulsed valve, laser(s) and oscilloscope or camera system is achieved with a delay generator (SRS DG535).

III. RESULTS AND DISCUSSION

A. Internal-state distributions

The two upper traces in Fig. 3 show experimental one-colour (1+1)-REMPI spectra of incoming and scattered beam. The incoming beam (upper trace) shows two peaks, both originating from the + parity component of the $J=1$ level in the $a^3\Pi_1$ state. Ionization occurs via the $N=1$ and $N=3$ level in the $b^3\Sigma^+(v=0)$ state, respectively. The absence of the $N=0$ and $N=2$ peak indicates that the electric fields used in the extraction region (below 10 V/cm), are not high enough to induce mixing of the two Λ-doublet components of the $J=1$ level.

The high laser power that is used guarantees complete saturation of the allowed b←a transition. In the analysis of the spectrum of incoming and scattered beam, the Hönl–London factors of the b←a transition can therefore be omitted. The ionization step is not saturated, and the (1+1)-

REMPI signal depends therefore linearly on laser power. The spectra are corrected for intensity fluctuations in the metastable CO beam and energy of the ionization laser. The peaks in the upper trace of the figure have equal intensity, as they both originate from the same level in the $a^3\Pi$ state.

The observed (1+1)-REMPI spectrum of the scattered CO molecules, shown in the middle trace of Fig. 3, yields the internal state distribution of the scattered metastable CO molecules. This spectrum is recorded for a mixture of 20% CO seeded in Ar at an angle of incidence $\theta_i = 51°$. The spectrum is observed to be much more dense than the spectrum of the incoming beam, indicating a strong redistribution within the $a^3\Pi$ state upon collision with the LiF(100) surface. The number of ions that is produced in the scattered beam is, on top of the strongest bandhead, approximately a factor of 200 smaller than the number of ions that are produced when molecules of the incoming beam are probed.

The lower trace in Fig. 3 shows the best fit to the experimental spectrum, using a least-squares intensity fit of the entire spectrum. Frequencies of the transitions are obtained from literature[26,27] and are kept fixed in the fitting procedure. The intensity $I_{J,\Omega}$ of each line, used for fitting the experimental data, is calculated from the population in a specific $a^3\Pi_\Omega(J)$ level to be

$$I_{J,\Omega} = \left(\frac{c^2_{\Omega,0}(J) W_0}{N_0} + \frac{c^2_{\Omega,1}(J)}{N_1} + \frac{c^2_{\Omega,2}(J) W_2}{N_2} \right) (2J+1) \times \exp\left(- \frac{E_{J,\Omega}}{kT_{rot}} \right) \quad (1)$$

in which

$$N_\mathrm{i} = \sum_{\text{all levels}} c^2_{\Omega,\mathrm{i}}(J)(2J+1)\exp\left(- \frac{E_{J,\Omega}}{kT_{rot}} \right) \quad (2)$$

for i=0, 1 or 2. Hönl–London factors are omitted in the fit for the reasons explained above. The indicated quantum numbers J and Ω are those of the $a^3\Pi$ state. The value $c^2_{\Omega,\mathrm{i}}(J)$ represents the amount of $\Omega' = \mathrm{i}$ (i=0, 1, or 2) character in the wave function of the quantum state labeled by J and Ω[28]. $W_{0,2}$ is the relative weight of the total population in levels with $\Omega = 0$ or 2 character with respect to the total population of levels with $\Omega = 1$ character. $E_{J,\Omega}$ is the energy of the specific (J, Ω) level in the $a^3\Pi$ state. The population in levels with $\Omega = \mathrm{i}$ character is normalized by N_i (i=0, 1 or 2) which is the sum of the Boltzmann population

$$(2J+1)\exp\left(- \frac{E_{J,\Omega}}{kT_{rot}} \right)$$

over all levels weighted with the amount of $\Omega = \mathrm{i}$ character. The rotational temperature is given as T_{rot}.

Normally the rotational temperature is defined with respect to a certain Ω ladder, as for example can be done for NO in its electronic ground state.[29–31] In this electronic state, NO can be well described in the pure Hund's case (a) approximation for rotational levels up to $J = 20.5$. For higher rotational levels, mixing of the different Ω ladders will occur (determined by $Y = A/B = 72.5$), and the energy levels must be calculated in a description intermediate between Hund's case (a) and (b). For CO in the $a^3\Pi$ state ($Y = 24.6$), strong mixing of the different Ω ladders occurs already above $J = 5$, and Ω is no longer a good quantum number. Defining the population of a specific level as given in Eq. (1) attaches the rotational temperature not to a specific Ω ladder (which is only valid in the pure Hund's case (a) approximation where Ω is a good quantum number), but to the Ω character. This accounts for the increasingly mixed character of the wave function with increasing rotational quantum number.

TABLE I. For each of the carrier gases used, the rotational temperature and weight of the population of the $\Omega = 0$ and 2 character relative to the population of the $\Omega = 1$ ($W_{0,2}$) as obtained from the best fit to the experimental spectrum as well as the internal energy E_{int} that is gained in the collision with the surface (calculated from the fit parameters) is given (for $\theta_\mathrm{i} = 51°$ and a surface temperature of $T_s = 298$ K).

Carrier gas	T_{rot} (K)	W_0	W_2	E_{int} (meV)
Ne	360(30)	0.56(3)	0.49(3)	28(4)
Ar	293(25)	0.39(2)	0.40(2)	24(3)
Kr	330(25)	0.27(4)	0.47(5)	26(4)
Xe	243(20)	0.56(5)	0.57(6)	20(3)

A small fraction of the spectrum of the incoming beam had to be added to the scattered spectrum as well, probably caused by a few ions from the incoming beam appearing in the time gate centered on signal of the scattered beam.

A least-squares fit of the contour of the observed spectrum to Eq. (1) results in a rotational temperature $T_{rot} = 293 \pm 25$ K. Fitting the spin-multiplet components with three different rotational temperatures does not improve the fit significantly. Best agreement with experiment is obtained when a non-equilibrium distribution for the three Ω components is assumed; in the final state distribution there appears to be an overpopulation of the (initially prepared) $\Omega = 1$ component relative to both the $\Omega = 0$ and $\Omega = 2$ component, as can be seen from the values for W_i given in Table I. This table contains the rotational temperature and the values for W_i as obtained from the fit for all of the carrier gases, together with the corresponding gain in internal energy E_{int} with respect to the ($J = 1, \Omega = 1$)-level, as calculated using these parameters. The situation with $W_0 = W_2 = 0$ would correspond to conservation of $\Omega = 1$ character, while the situation with $W_0 = W_2 = 1$ corresponds to a completely (electronically and rotationally) thermalized Boltzmann-like distribution.

The rotational temperature tends to decrease with decreasing velocity of the incoming beam. The overpopulation of the initially prepared $\Omega = 1$ character is obvious for all of the carrier gases. Striking is the equal population of levels with $\Omega = 0$ and 2 character for almost all of the carrier gases.

B. Fluorescence profiles

Fluorescence profiles are measured for two different situations: the first is with the LiF(100) surface positioned in the molecular beam, the second with the molecular beam hitting the stainless steel sample holder under otherwise identical circumstances. Since stainless steel very efficiently

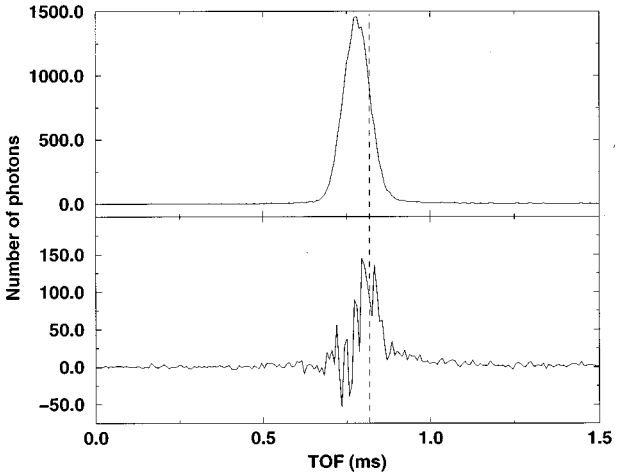

FIG. 4. Upper trace: Fluorescence profile of metastable CO obtained with the LiF sample placed in the molecular beam. The profile is recorded for a 20% CO in Ne mixture. Lower trace: Fluorescence profile obtained by taking the difference between the upper profile and a similar profile measured by replacing the LiF sample by the stainless steel sample holder under otherwise identical circumstances. Vertical dashed line: mean arrival time of incoming metastable CO beam at LiF surface.

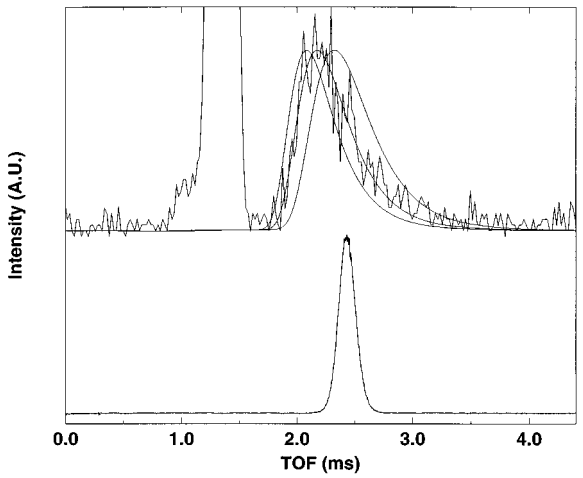

FIG. 5. Measured TOF profiles of both incoming (lower trace) and scattered (upper trace) metastable CO molecules for a mixture of 20% CO in Kr. On the horizontal axis the time relative to the laser preparation is indicated. The lower trace shows the measured TOF distribution of the incoming beam (the horizontal axis is rescaled to allow direct comparison with the scattered TOF distribution). The upper trace includes the scattered TOF distribution (second peak) and the best fit (T_{trans}=285 K) as well as calculated TOF profiles for T_{trans}=185 K (right) and 385 K (left). The first peak (off-scale) corresponds to spontaneous fluorescence of the laser-prepared metastable molecules.

deexcites the metastable CO molecules via an Auger process, in which the internal energy of the CO molecules is used to emit an electron from the surface,[32] the fluorescence profile measured with this target in the molecular beam only shows fluorescence caused by metastable CO molecules in the incoming beam. The difference signal between profiles measured with LiF(100) and stainless steel target provides the fluorescence signal of the scattered metastable CO molecules. The profiles are measured for a mixture of 20% CO seeded in neon, because the survival probability for faster molecules is larger (*vide infra*).

The upper trace of Fig. 4 shows the fluorescence signal as obtained for the first situation. The horizontal axis shows the time after laser excitation. The vertical axis shows the number of counted photons. The lower trace represents the (noisy) difference signal between the situation with LiF target and stainless steel target. The vertical dashed line shows the mean arrival time of the incoming beam at the position of the LiF surface. At this time a small, 150-μs-wide peak is observed. The height of this peak is a direct measure for the upper limit of the survival probability.

Because the internal state distribution of the scattered molecules is probed as well (see the previous section), the time evolution of the fluorescence profile of the scattered metastable CO molecules can be calculated by summing the exponentially decaying curves for each of the populated levels. This is done because the lifetime in the $a^3\Pi$ state is strongly dependent on rotational- and Ω-quantum number.[33] The (integrated) intensity of each exponential is weighted with the population of the specific quantum state. From the calculated fluorescence profile it is deduced that, for a typical distribution of population as deduced from the REMPI experiments (the parameters to obtain this distribution are listed in Table I), the fluorescence yield of scattered metastable CO molecules is a factor of 2.5 smaller than the fluorescence yield of metastable CO molecules in the incoming beam. Taking the effect of the change in fluorescence yield into account, the upper limit for the survival probability is calculated to be $(18\pm 8)\%$.

Because the signal peak in the lower trace coincides with the arrival time of the incoming beam and has a width comparable to the TOF distribution of the incoming beam (see the next section), it is tempting to state that this peak can (at least partly) be explained by enhanced fluorescence, caused by the interaction of the CO molecule with the LiF surface. Assuming the entire peak to be explained by this mechanism, the efficiency of deexcitation via this mechanism is still only on the order of 10^{-4} of the total amount of incoming molecules. The broad background signal that is observed at larger flight times, however, must be explained by fluorescence signal of scattered molecules anyway.

C. Time-of-flight profiles

Figure 5 shows the TOF profiles of both incoming and scattered metastable CO molecules as measured for a 20% CO in Kr mixture. In the lower trace the TOF profile of the metastable CO molecules impinging on the LiF surface, as detected with the MCP (Fig. 1), is shown. The corresponding velocity distribution has a width (full width at half-maximum) of less than 10% of the mean velocity. The time axis of the lower trace is rescaled to correspond to a flight path (72.5 cm+50 cm) which is identical to the flight path that the scattered metastable CO molecules must travel to reach the MCP/phosphor screen combination (Fig. 2a). This allows direct comparison of the TOF distributions of incoming and scattered metastable CO molecules as shown in Fig. 5.

The first peak (off scale) in the upper trace in Fig. 5 is due to the fluorescence of metastable CO molecules decaying to the electronic ground state; the detected fluorescence is emitted in the direction of the MCP detector by molecules that are passing through the field of view of this detector from the moment that they enter the UHV chamber until they hit the LiF surface. The origin of this peak is confirmed by installing a Suprasil 1 window in front of the MCP detector. In this setup the fluorescence peak was still present, while even at the maximum of the scattered metastable signal no significant amount of fluorescence signal was visible. The time-integrated fluorescence signal is a direct measure for the amount of incoming molecules.

The second peak in the upper trace corresponds to the TOF distribution of the scattered molecules. This peak is clearly broader than the distribution of the incoming beam (lower trace) and has a tail to larger flight times. The profile of scattered CO molecules is fitted to the convolution of the measured velocity distribution of the incoming beam at the position of the LiF surface (as can be calculated by rescaling the time axis to correspond to the flight path needed to reach the LiF surface, which is 72.5 cm) and a Maxwellian velocity distribution. In thermal equilibrium, the number of molecules with absolute velocity between v and $v+dv$ is given by

$$f(v)dv = Cv^2 \exp\left(-\frac{mv^2}{2kT_{trans}}\right)\exp\left(-\frac{A}{v}\right)dv. \qquad (3)$$

The first two terms describe a Maxwellian velocity distribution with a Boltzmann temperature T_{trans} whereas the last term is included to take the velocity dependent survival probability (*vide infra*) into account. The factor C is a normalization constant. From this velocity distribution it is calculated that the number of molecules that will reach the surface of the MCP detector in a time interval between t and $t+dt$ is given by:[34,35]

$$F(t)dt = C't^{-4}\exp\left(-\frac{m(l/t)^2}{2kT_{trans}}\right)\exp\left(-\frac{At}{l}\right)dt, \qquad (4)$$

where l is the distance between surface and detector and C' is a normalization constant. The convolution is performed in the time domain. The best fitting curve, with $T_{trans}=285$ K, is superimposed on the experimental trace of Fig. 5. For comparison, also traces with translational temperatures of 185 K (right peak) and 385 K (left peak) are indicated in the figure. It should be noted that the effect of the finite lifetime of the scattered metastable CO molecules on the TOF distributions of the scattered CO molecules, as described above for the fluorescence profiles, should in principle be accounted for in the analysis as well [the lifetime of the $J=1$ level in the $\Omega=1$ ladder is around 3 ms, lifetimes of other levels are all (much) larger than this value].[33] Neglecting the finite lifetime, however, barely influences the determination of the Boltzmann temperature.

In many cases a shifted Maxwell velocity distribution with a drift velocity is fitted to the experimental TOF profiles. Since the fit is already almost perfect, adding an extra fit parameter would not significantly improve the fit and would give unreliable results because of the strong coupling between the drift velocity and the translational temperature.

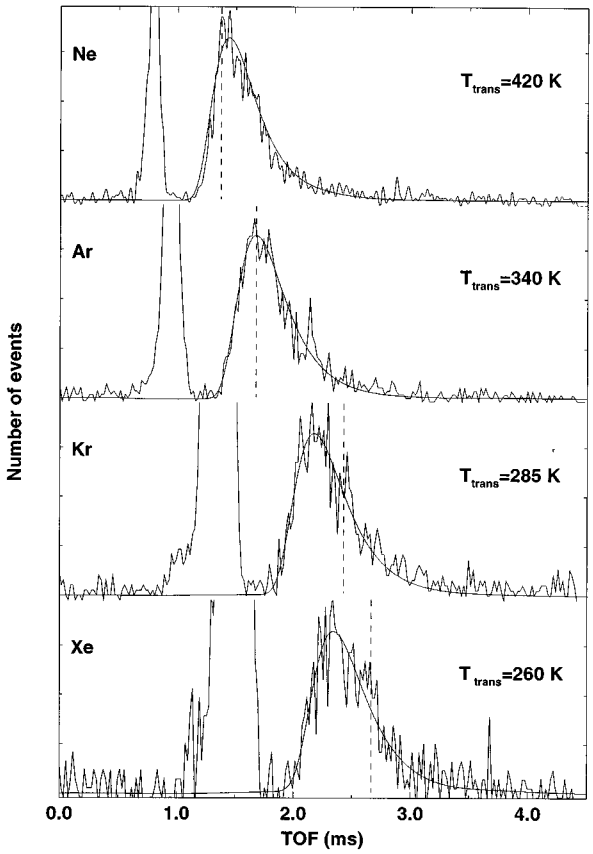

FIG. 6. Measured TOF profiles of scattered metastable CO molecules for mixtures of 20% CO in Ne, Ar, Kr and Xe. The best fit is superimposed upon the experimental traces. The dashed line, indicated for each of the TOF profiles, shows the averaged arrival time for a completely elastic scattering process, as obtained from the TOF distribution of the incoming beam.

All TOF measurements have been performed for four different carrier gases, i.e., for four different incoming velocities. The results are displayed in Fig. 6. The best fits to these profiles are superimposed on the experimental traces. For each of these fitted profiles the average velocity v_{in} and kinetic energy E_{in} of the incoming beam, the best fitting Boltzmann temperature T_{trans}, and the corresponding averaged velocity (v_{det}) and kinetic energy (E_{det}) of the outgoing beam as present on the detector, are listed in Table II.

TABLE II. For each of the carrier gases used, the averaged velocity v_{in} and averaged kinetic energy E_{in} of the incoming beam, the best fitting Boltzmann temperature T_{trans} and the corresponding averaged velocity v_{det} and kinetic energy E_{det} of the outgoing beam at the detector are given (all for $\theta_i=36°$ and a surface temperature of $T_s=298$ K).

Carrier gas	v_{in} (m/s)	E_{in} (meV)	T_{trans} (K)	v_{det} (meV)	E_{det} (meV)
Ne	884(9)	113.8(12)	420(30)	722(22)	83(5)
Ar	732(7)	77.8(8)	340(35)	660(30)	69(6)
Kr	504(5)	36.9(4)	285(50)	613(45)	59(9)
Xe	461(4)	31.0(3)	260(55)	593(50)	55(10)

The dashed lines in Fig. 6 indicate the averaged arrival time, obtained from the TOF distribution of the incoming beam assuming a completely elastic scattering process. From comparing the TOF profiles of the scattered metastable CO molecules to the averaged arrival time for completely elastic scattering it is concluded that for CO seeded in Ne the scattered beam is slower than the incoming beam. This is the expected behavior for a superthermal molecular beam scattering from a room temperature surface. For CO seeded in Ar the incoming beam and the scattered beam are (almost) equally fast. For CO seeded in Kr and Xe, the scattered molecules are significantly faster than molecules in the incoming beam. This apparent acceleration is caused by the velocity dependent survival probability (see below), that is taken into account by the last exponential in Eqs. 3 and 4. This effect is also clear from the data listed in Table II: it is seen that E_{det} is superthermal (>37.5 meV) for all of the carrier gases used and that for CO seeded in Kr and Xe the averaged velocity of the scattered molecules is larger than the averaged kinetic energy of the incoming beam. Because faster molecules have a larger probability to survive the collision with the surface as a metastable molecule than slower molecules (see below), this leads to a velocity distribution of the detected scattered molecules that is skewed to larger velocities.

The translational temperature as obtained from the fit is seen to decrease gradually in going from Ne to Xe and this shows that the velocity distribution of the scattered molecules is not completely accommodated to the surface. The translational temperature is (within error) independent of the azimuthal angle (for non-specular scattering). It is noted that the angle of incidence for the determination of the rotational temperature is different from the angle used for measuring the translational temperature. Because the averaged impact energy is different, direct comparison of these temperatures is impossible, although they show a similar trend.

The ratio of the integrated scattered metastable CO signal to the product of the integrated fluorescence signal with v_{in} is presented in Fig. 7 (circles with error bars) for each of the carrier gases used. This number is a measure for the survival probability (SP). It is seen from the data that the relative SP is decreasing with a decrease of the velocity of the incoming CO molecules.

The measured velocity dependence of the SP can, in a simple model, be used to quantitatively determine the SP. In this model the SP at the surface is assumed to be exponentially decaying with the interaction time with the surface, where the latter is taken to be proportional to $(1/v_{in}+1/v_{out})$. The quantity v_{out} is obtained using Eq. (3), the best fitting translational temperature, and omitting the velocity dependent survival probability from this expression. In Fig. 7 $1/v_{in}+1/v_{out}$ is plotted on the horizontal axis. Fitting the experimentally determined relative survival probabilities to this model determines the value of A in Eq. (3) and yields the absolute survival probabilities for the various carrier gases (assuming the boundary conditions that a zero interaction time gives a SP of 1, and an infinite interaction time gives a SP of 0). The vertical axis of Fig. 7 is rescaled to correspond to the absolute survival probability as obtained from the fit (indicated by the solid line in the figure). Because the translational temperature (and thus the velocity in the outgoing channel v_{out}) and A are coupled to each other, a few iteration cycles have been performed to determine the stable values of A and T_{trans}.

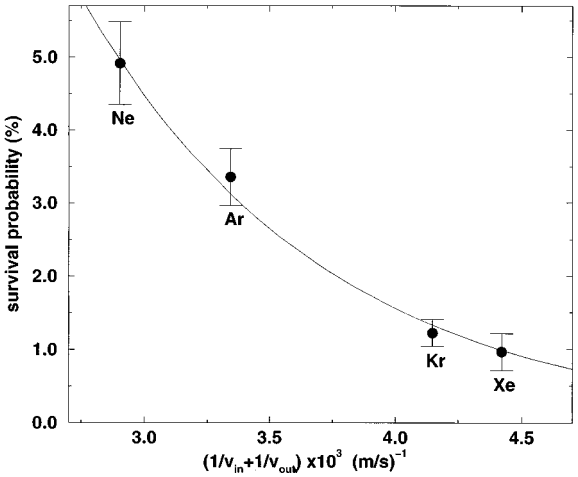

FIG. 7. The circular points (with error bar) represent the relative survival probability for the carrier gases used. The value plotted on the horizontal axis $(1/v_{in}+1/v_{out})$ is, in approximation, proportional to the residence time on the surface for scattering at specular angles. The smooth curve shows the best fit to the experimental data points, allowing the determination of absolute survival probability. The vertical axis is rescaled to correspond to the absolute survival probability as obtained from this fit.

D. Angular distributions

The angular distributions are measured with the MCP/phosphor screen combination as indicated in Fig. 2d. A typical grey scale image measured with this detector is given in Fig. 8 for a mixture of 20% CO in Ar and an angle of incidence of $\theta_i=60°$. The angular distribution is obtained by using 2D event counting and summing over typically 1.5 $\times 10^5$ laser shots. Both in-plane and out-of-plane scattering angles are indicated in the figure. The distribution of scattered metastable CO molecules is observed to be very broad, both in plane and out of plane. The ''hole'' that is visible in the middle of this image is caused by the bias angle of the channels in the MCP which causes an angular dependent detection efficiency; metastable molecules coming in under the bias angle penetrate the channels and are detected less efficiently. By moving the sample relative to the 2D-imaging detector, this hole in the distribution can be moved out of the images; the angular distribution of the scattered molecules is accurately determined if the sample is moved over a distance of 1 cm in the direction of the excitation region.

Figure 9 shows the in-plane angular distribution that is obtained by taking a horizontal profile of such a 2D image (circular dots), corrected for all effects concerning solid angle of detection and pixel size. The horizontal axis is rescaled to correspond to the scattering angle θ_f. The smooth curve indicated in the figure shows a cosine distribution, the best fit to the experimental data points. Squared and cubed

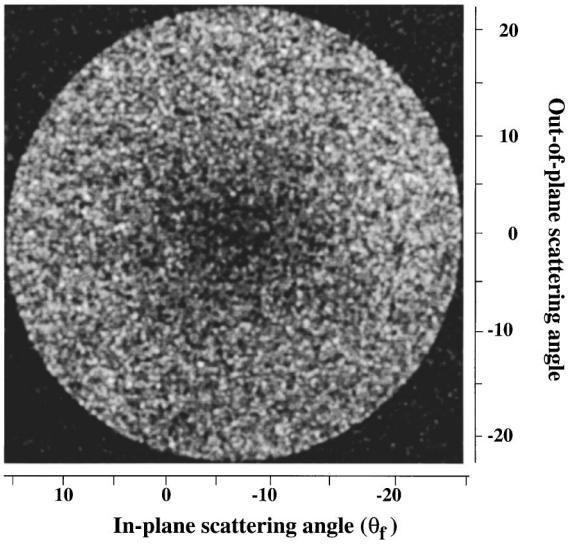

FIG. 8. Two-dimensional grey scale image of the angular distribution ($\theta_i = 60°$) of the metastable CO molecules taken with MCP 3. The ''hole'' in the distribution in the middle of the MCP is a result of the bias angle of the channels leading to an angle-dependent reduction in sensitivity of the MCP detection system.

cosine distributions do not fit the experimental data as well. The deviation of the experimental data points from the cosine curve for lower scattering angles can again be explained by the angular dependent sensitivity of the MCP detector. Similar experiments have also been performed for all the other carrier gases and show an equally broad, cosine-like angular distribution.

For a direct scattering process, generally the parallel momentum is conserved and the angular distribution of the scattered molecules is close to specular[1]. The broad angular distribution on itself might indicate a trapping-desorption mechanism, but as trapping of the metastable molecules is most probably followed by electronic deexcitation this is not very likely to happen. In the scattering of metastable rare gas atoms from LiF(100) surfaces it has also been found that the

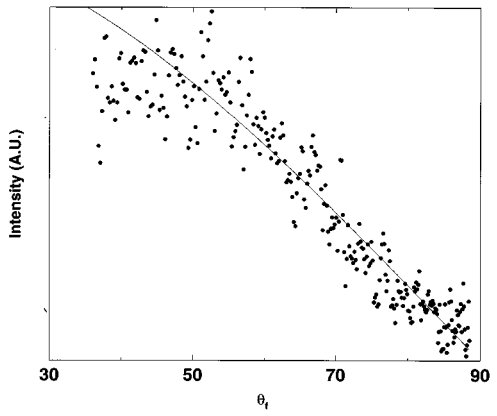

FIG. 9. In-plane angular distribution of scattered metastable CO molecules, as obtained from a 2D image as shown in Fig. 8. The circular points show the experimental data as obtained for a mixture of 20% CO in Ar, and an angle of incidence $\theta_i = 33°$. The smooth curve shows a cosine distribution.

angular distributions are much wider than those of the respective ground state atoms[36], which is attributed to the marked change in interaction potential. Also in our case the broad angular distributions might be caused by the detailed character of the molecule-surface interaction potential; LiF is an ionic crystal, and the large dipole moment of the metastable CO molecules (1.37 D[37]) will interact with the various Li(+)-F(−) dipoles at the surface. Since LiF is a cubic crystal, these surface dipoles are both in the horizontal and the vertical direction, inducing not only a broad in-plane distribution but also a very broad out-of-plane distribution.

IV. CONCLUSIONS

In this paper we have presented state-to-state scattering experiments with laser-prepared metastable molecules. The survival of electronically excited, state-selected CO molecules, colliding with a cleaved LiF(100) surface, is analyzed using time- and spatially resolved detection techniques. The absolute survival probability for metastable CO scattering from LiF(100) is observed to be between 1 and 5% for the conditions used in the experiments, consistent with the upper limit of 18% obtained from the fluorescence profiles. A clear increase of the survival probability with an increasing velocity is observed.

The translational temperature, obtained from the TOF profiles of the surviving metastable CO molecules, shows that the metastable CO molecules are scattered from the surface with incompletely thermalized velocities. The rotational temperature shows a similar trend and it is concluded therefore that the metastable CO molecules undergo direct inelastic scattering. The population in the initially prepared $\Omega = 1$ character is larger than the population in the other spin components.

The angular distributions are observed to be broad which might be attributed to the strong corrugation of the electrostatic interaction potential in the CO*/LiF(100) system.

ACKNOWLEDGMENTS

We thank Carsten Menzel for fruitful discussion and preparation of the LiF crystals, J. Gerritsen for characterizing the LiF surfaces and C.A. Sikkens, J.G.H. Hermsen and C.A. Timmer for technical support. This work has been realized in the framework of the EC-HCM network (ERB-CHR-XCT-94-0603).

[1] J. A. Barker and D. J. Auerbach, Surf. Sci. Rep. **4**, 1 (1984).
[2] *Atomic and Molecular Beam Methods*, edited by G. Scoles (Oxford University Press, New York, 1988/1992), Vols. I and II.
[3] C. W. Mulhausen, J. A. Serri, J. C. Tully, G. E. Becker, and M. J. Cardillo, Isr. J. Chem. **22**, 315 (1982).
[4] A. W. Kleyn, A. C. Luntz, and D. J. Auerbach, Phys. Rev. Lett. **47**, 1169 (1981).
[5] E. W. Kuipers, M. G. Tenner, and A. W. Kleyn, Nature **334**, 420 (1988).
[6] D. A. Mantell, S. B. Ryali, G. L. Haller, and J. B. Fenn, J. Chem. Phys. **78**, 4250 (1983).
[7] M. Asscher, W. L. Guthrie, T.-H. Lin, and G. A. Somorjai, Phys. Rev. Lett. **49**, 76 (1982).
[8] J. Misewich, C. N. Plum, G. Blyholder, P. L. Houston, and R. P. Merill, J. Chem. Phys. **78**, 4245 (1983).

[9] H. Zacharias, M. M. T. Loy, and P. A. Roland, Phys. Rev. Lett. **49**, 1790 (1982).
[10] M. Gostein, H. Parhikhteh, and G. O. Sitz, Phys. Rev. Lett. **75**, 342 (1995).
[11] J. Misewich, H. Zacharias, and M. M. T. Loy, Phys. Rev. Lett. **55**, 1919 (1985).
[12] A. C. Luntz, A. W. Kleyn, and D. J. Auerbach, Phys. Rev. B **25**, 4273 (1982).
[13] G. D. Kubiak, J. E. Hurst, H. G. Rennagel, G. M. McClelland, and R. N. Zare, J. Chem. Phys. **79**, 5163 (1983).
[14] D. A. Mantell , Y.-F. Maa, S. B. Ryali, G. L. Haller, and J. B. Fenn, J. Chem. Phys. **78**, 6338 (1983).
[15] W. Sesselmann, H. Conrad, G. Ertl, J. Küppers, B. Woratschek, and H. Haberland, Phys. Rev. Lett. **50**, 446 (1983).
[16] W. Maus-Friedrichs, S. Dieckhoff, and V. Kempter, Surf. Sci. **249**, 149 (1991).
[17] R. T. Jongma, G. Berden, D. v.d. Zande, T. Rasing, H. Zacharias, and G. Meijer, Phys. Rev. Lett. **78**, 1375 (1997).
[18] R. T. Jongma, Th. Rasing, and G. Meijer, J. Chem. Phys. **102**, 1925 (1995).
[19] R. W. Field, S. G. Tilford, R. A. Howard, and J. D. Simmons, J. Mol. Spectrosc. **44**, 347 (1972).
[20] K. H. Kramer and R. B. Bernstein, J. Chem. Phys. **42**, 767 (1965).
[21] J. Estel, H. Hoinkes, H. Kaarmans, H. Nahr, and H. Wilsch, Surf. Sci. **54**, 393 (1976).
[22] R. Hemmen and H. Conrad, Phys. Rev. Lett. **67**, 1314 (1991).
[23] M. R. Woodard, R. C. Sharp, M. Seely, and E. E. Muschlitz, J. Chem. Phys. **69**, 2978 (1978).
[24] B. Brutschy and H. Haberland, Phys. Rev. A **19**, 2232 (1979).
[25] W. L. Borst, G. Nowak, and J. Fricke, Phys. Rev. A **17**, 838 (1978).
[26] G. H. Dieke and J. W. Mauchly, Phys. Rev. **43**, 12 (1933).
[27] T. Rytel, J. Mol. Spectrosc. **145**, 420 (1991).
[28] The values for $c^2_{\Omega',i}(J)$ are calculated using the model of Field *et al.* (Ref. 19) to determine the energy of rotational levels in the $a^3\Pi$ state. In this model all the Ω ladders are interacting with each other. From the wave function belonging to the specific quantum state labeled by J and Ω', the amount of $\Omega=i$ character is calculated.
[29] A. E. Wiskerke, C. A. Taatjes, A. W. Kleyn, R. J. W. E. Lahaye, S. Stolte, D. K. Bronnikov, and B. E. Hayden, Chem. Phys. Lett. **216**, 93 (1993).
[30] K. Fukutani, Y. Murata, R. Schwarzwald, and T. J. Chuang, Surf. Sci. **311**, 247 (1994).
[31] A. E. Wiskerke, C. A. Taatjes, A. W. Kleyn, R. J. W. E. Lahaye, S. Stolte, D. K. Bronnikov, and B. E. Hayden, J. Chem. Phys. Lett. **102**, 3835 (1995).
[32] H. D. Hagstrum, Phys. Rev. **96**, 336 (1954).
[33] T. C. James, J. Chem. Phys. **55**, 4118 (1971).
[34] P. M. Ferm, F. Budde, A. V. Hamza, S. Jakubith, G. Ertl, D. Weide, P. Andresen, and H.-J. Freund, Surf. Sci. **218**, 467 (1989).
[35] F. Budde, T. Gritsch, A. Mödl, T. J. Chuang, and G. Ertl, Surf. Sci. **178**, 798 (1986).
[36] H. Conrad, G. Ertl, J. Küppers, W. Sesselmann, B. Woratschek, and H. Haberland, Surf. Sci. **117**, 98 (1982)
[37] R. C. Stern, R. H. Gammon, M. E. Lesk, R. S. Freund, and W. A. Klemperer, J. Chem. Phys. **52**, 325 (1970).